CHAPTER II
LITERATURE REVIEW

2.1. Azo Dyes

2.1.1 General Remarks

The term of "azo dyes" is applied to those synthetic organic colorants that are characterized by the presence of the chromophoric azo group ($-N=N-$). This divalent group is attached to sp^2 hybridized carbon atom on one side and to an aromatic or heterocyclic nucleus on the other. It may be linked to an unsaturated molecule of the carboxylic, heterocyclic, or aliphatic type. No natural dyes contain this chromophore. Commercially, the azo dyes are the largest and most versatile class of organic dyestuffs. There are more than 10,000 Color Index (CI) generic names assigned to commercial colorants, where approximately 4,500 are in use, and over 50% of these belong to the azo class. Synthetic dyes are derived in whole or in part from cyclic intermediates. Approximately two-thirds of the dyes are used by the textile industry to dye natural and synthetic fiber or fabrics, about one-sixth is used for coloring paper, and the rest is used chiefly in the production of organic pigments and in the dyeing of leather and plastic. Dye are sold as pastes, powders, and liquids with concentrations varied from 6 to 100%. The concentration, form, and purity of a dye are determined largely by the use, for which it is intended.

2.1.2 Classification and Designations

The most authoritative compilation covering the constitution, properties, preparations, manufactures, and other coloring data is the publication of Color Index, which is edited jointly by the Society of Dyers and Colorists and the American Association of Textile Chemists and Colorists (AATCC). In the Color Index, a dual classification system is employed to group dyes according to area of usage and chemical constitution. Because of the ease of applications, azo dyes comprise the largest chemical class in numbers, monetary value, and tonnage produced. There are more than 2,200 chemical structures of azo dyes disclosed in the Colour Index.

Nearly all dye manufactures use letters and numerals in the name of their products to define the color. Thus, B is blue; G, yellow (gelb in German) or green; R, red; and Y, yellow. Numerals, i.e. 2G (or GG), 3G, 4G, etc. indicate, in this case, a successively yellower or greener shade. Occasionally, suffixed letters are used to feature other properties, such as solubility, light fastness, brightness, and use on synthetic fibers.

Chemically, the azo class is subdivided according to the number of azo groups present into mono-, dis-, tris-, tetrakis-, etc. Mono- and diazo dyes are essentially equal in importance, trisazo dyes are less important, and tetrakisazo dyes, except for a few, are much less important. For this reason, substances with more than three azo linkages are generally included under the heading of polyazo dyes. Table 1 lists the Color Index of the azo dyes.

Table 2.1 Color Index of different azo dyes (Mary, H. G., 1991)

Chemical class	Color Index number range
Monoazo	11,000 – 19,999
Diazo	20,000 – 29,999
Trisazo	30,000 – 34,999
Polyazo	35,000 – 36,999

2.2. Semiconductor

A semiconductor is a material with an electrical conductivity that is intermediate between that of an insulator and a conductor. Like other solids, semiconductor materials have electronic band structure determined by the crystal properties of the material. A semiconductor used as photocatalyst should be an oxide or sulfide of metals, such as TiO_2, CdS, and ZnO. The actual energy distribution among electrons is described by the Fermi level and temperature of the electrons. At absolute zero temperature, all of the electrons have energy below the Fermi energy, but at non-zero temperature, the energy levels are randomized, and some electrons have energy above the Fermi level.

Among the bands filled with electrons, the one with the highest energy level is referred to as the valence band, and the band outside of this is referred to as the conduction band. The energy width of the forbidden band between the valence band and the conduction band is referred to as the band gap. The overall structure of band gap energy is shown in Figure 2.1.
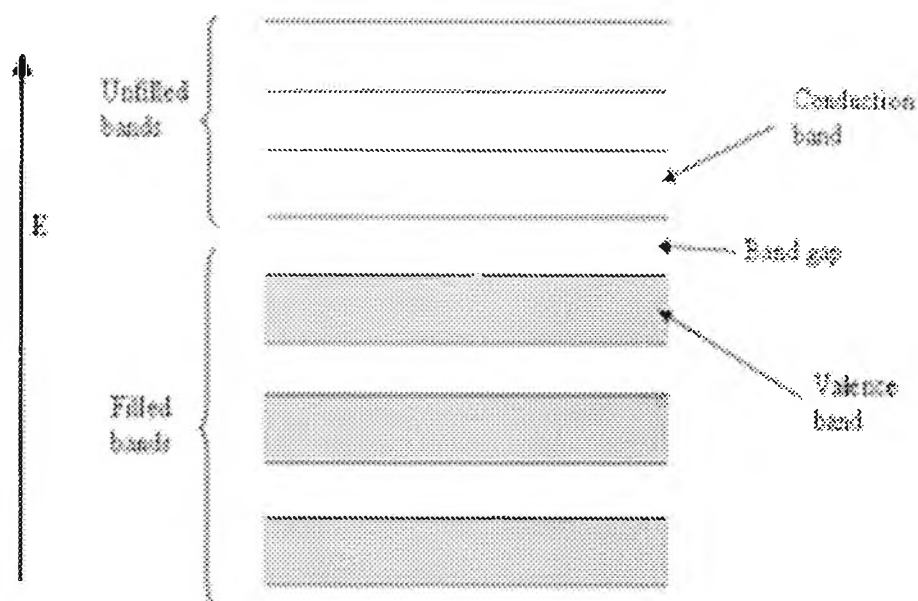

Figure 2.1 The structure of band gap energy.

The band gap can be considered as a wall that electrons must jump over in order to become free. The amount of energy required to jump over the wall is referred to as the band gap energy (E_g). Only electrons that jump over the wall and enter the conduction band (CB, which are referred to as conduction band electrons) can move around freely. When light is illuminated at appropriate wavelengths with energy equal or more than band gap energy, valence band (VB) electrons can move up to the conduction band (CB). At the same time, as many positive holes as the number of electrons that have jumped to the conduction band (CB) are created. The valence band (VB), conduction band (CB), band gap, and band gap wavelength of some common semiconductors are shown in Table 2.1.

Table 2.2 The band gap positions of some common semiconductor photocatalysts (Robertson, 1996)

Semiconductor	Valence band (eV)	Conduction band (eV)	Band gap (eV)	Band gap wavelength (nm)
TiO_2	+3.1	-0.1	3.2	387
SnO_2	+4.1	+0.3	3.8	326
ZnO	+3.0	-0.2	3.2	387
ZnS	+1.4	-2.3	3.7	335
WO_3	+3.0	+0.2	2.8	443
CdS	+2.1	-0.4	2.5	496
CdSe	+1.6	-0.1	1.7	729
GaAs	+1.0	-0.4	1.4	886
GaP	+1.3	-1.0	2.3	539

2.3. Titanium Oxide Photocatalyst

2.3.1 General remarks

Titanium dioxide (TiO_2) belongs to the family of transition metal oxides. TiO_2 has received a great deal of attention due to its chemical stability, non-toxicity, low cost, and other advantageous properties. Particularly, TiO_2 is extensively utilized in solar energy conversion, i.e. solar cell and photocatalysis applications (Hoffmann et al., 1995). As a result of its high refractive index, it is used as anti-reflection coating in silicon solar cells and in many thin film optical devices. TiO_2 is successfully used as gas sensor due to the dependence of the electric conductivity on the ambient gas composition and is utilized in the determination of oxygen and carbon monoxide concentrations at high temperatures (> 600°C), and simultaneously determining CO/O_2 and CO/CH_4 concentrations (Savage et al., 2001). Due to its hemocompatibility with the human body, TiO_2 is also used as a biomaterial (as bone substituent and reinforcing mechanical supports).

2.3.2 Crystal structure and properties

The main four polymorphs of TiO_2 found in nature are anatase (tetragonal), brookite (orthorhombic), rutile (tetragonal), and TiO_2 (B) (monoclinic). The structures of rutile, anatase, and brookite can be discussed in terms of (TiO_2^{6-}) octahedrals. The three crystal structures differ by the distortion of each octahedral and by the assembly patterns of the octahedral chains. Anatase can be regarded to be builtup from octahedrals that are connected by their vertices, in rutile, the edges are connected, and in brookite, both vertices and edges are connected, as shown in Figure 2.2 (Carp et al., 2004).
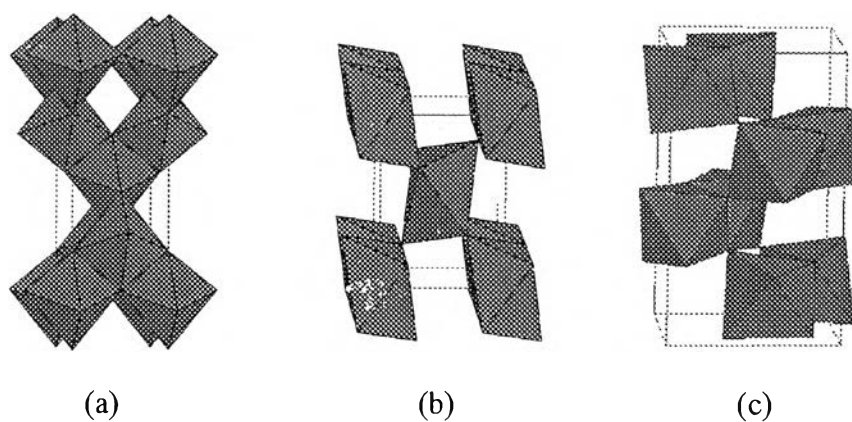

(a)   (b)   (c)

Figure 2.2 Crystal structures of (a) anatase, (b) rutile, and (c) brookite.

Thermodynamic calculations based on calorimetric data predict that rutile is the most stable phase at all temperatures and pressures up to 60 kbar. The small differences in the Gibbs free energy (4-20 kJ/mol) among the three phases suggest that the metastable polymorphs are almost as stable as rutile at normal pressures and temperatures. Particle size experiments affirm that the relative phase stability may reverse when particle sizes decrease to sufficiently low values due to surface energy effects (surface free energy and surface stress, which depend on particle size). If the particle sizes of the three crystalline phases are equal, anatase is the most thermodynamically stable at sizes less than 11 nm, brookite is the most stable between 11 and 35 nm, and rutile is the most stable at sizes greater than 35 nm (Zhang et al., 2000).

The enthalpy of the anatase-rutile phase transformation is low. However, there are widespread disagreement in the value, which ranges from -1.3 to -6.0 ± 0.8 kJ/mol. Kinetically, anatase is stable, i.e. its transformation into rutile at room temperature is so slow that the transformation practically does not occur. At macroscopic scale, the transformation reaches a measurable speed for bulk TiO_2 at temperature greater than 600°C. During the transformation, anatase pseudoclose-packed planes of oxygen are retained as rutile close-packed planes, and a co-operative rearrangement of titanium and oxygen ions occurs within this configuration. The proposed mechanism implies at least spatial disturbance of the oxygen ion framework and a minimum breaking of Ti–O bonds as a result of surface nucleation and growth. The nucleation process is very much affected by the interfacial contact in nanocrystalline solids, and once initiated, it quickly spreads out and grain growth occurs (Ding et al., 1998).

The anatase-rutile transformation has been studied for both mechanistic and application-driven reasons because the TiO_2 phase (i.e. anatase or rutile) is one of the most critical parameters determining the use as a photocatalyst, catalyst, or as ceramic membrane material. This transformation, achieved by increased temperature or pressure, is influenced by several factors, such as concentration of lattice and surface defects, particle size, and applied temperature and pressure.

In photocatalysis applications, both crystal structures, i.e. anatase and rutile, are commonly used, with anatase showing a greater photocatalytic activity for most reactions. It has been suggested that this increased photoreactivity is due to anatase's slightly higher Fermi level, lower capacity to adsorb oxygen, and higher degree of hydroxylation (i.e. number of hydroxyl groups on the surface). Reactions, in which both crystalline phases have the same photoreactivity (Deng et al., 2002) or rutile a higher one, (Mills et al., 2003) are also reported. Furthermore, there are also studies, which claim that a mixture of anatase (70-75%) and rutile (30-25%) is more active than pure anatase (Mugglie et al., 2001). The disagreement of the results may lie in the intervening effect of various coexisting factors, such as specific surface area, pore size distribution, crystal size, and preparation methods, or in the way the

activity is expressed. The behavior of Degussa P-25 commercial TiO_2 photocatalyst, consisting of a mixture of anatase and rutile in an approximate proportion of 80/20, is for many reactions more active than both the pure crystalline phases. The enhanced activity arises from the increased efficiency of the e^-/h^+ separation due to the multiphase nature of the particles.

2.3.3 Semiconductor characteristic and photocatalytic activity

Due to oxygen vacancies, TiO_2 is an n-type semiconductor. A semiconductor photocatalyst is characterized by its capability to adsorb simultaneously two reactants, which can be reduced and oxidized by a photonic activation through an efficient absorption ($hv \geq E_g$). The ability of a semiconductor to undergo photoinduced electron transfer to an adsorbed particle is governed by the band energy positions of the semiconductor and the redox potential of the adsorbates. The energy level at the bottom of conduction band is actually the reduction potential of photoelectrons. The energy level at the top of valence band determines the oxidizing ability of photogenerated holes, each value reflecting the ability of the system to promote reductions and oxidations. The flat band potential (V_{fb}) locates the energy of both charge carriers at the semiconductor-electrolyte interface, depending on the nature of the material and system equilibrium. From the thermodynamic point of view, adsorbed couples can be reduced photocatalytically by conduction band electrons if they have more positive redox potentials than V_{fb} of the conduction band, and can be oxidized by valence band holes if they have more negative redox potentials than V_{fb} of the valence band (Rajeshwar, 1995).

Unlike metals, semiconductors lack a continuum of interband states to assist the recombination of electron-hole (e^-/h^+) pairs, which assure a sufficiently long life time of the pairs to diffuse to the photocatalyst surface and initiate a redox reduction. The differences in lattice structures of anatase and rutile TiO_2 cause different densities and electronic band structures, leading to different band gaps (for bulk materials: anatase 3.20 eV and rutile 3.02 eV). Therefore, the absorption thresholds correspond to wavelengths of approximately 384 and 410 nm for the two TiO_2 forms, respectively. The mentioned values concern single crystals or well-crystallized samples. Higher values are usually obtained for weakly crystallized thin

films or nanosized materials. The blue shift of the fundamental absorption edge in TiO_2 nanosized materials has been observed amounting to 0.2 eV for crystallite sizes in the range of 5-10 nm.

2.4. Nano-Photocatalysts

2.4.1 General remarks

Nanocrystalline photocatalysts are ultra-small semiconductor particles, which are few nanometers in size. During the past decade, the photochemistry of nanosized semiconductor particles has been one of the fastest growing research areas in physical chemistry. The interest in these small semiconductor particles originates from their unique photophysical and photocatalytic properties. Several review articles have been published concerning the photophysical properties of nanocrystalline semiconductors. Such studies have demonstrated that some properties of nanocrystalline semiconductor particles are in fact different from those of bulk materials.

Nanosized particles possess properties with falling into the region of transition between the molecular and bulk phases. In the bulk material, the electron excited by light absorption funds a high density of states in the conduction band, where it can exist with different kinetics energies. In the case of nanoparticles, however the particle size is the same as or smaller than the size of the first excited state. Thus, the electrons and holes generated upon illumination cannot suit into such a particle, unless they assume a state of higher kinetics energy.

Hence, as the size of the semiconductor particle is reduced below a critical diameter, the spatial confinement of the charge carriers within a potential well, like "a particle in a box", causes them to mechanically behave quantum. In solid state terminology, this means that the bands split into discrete electronic states (quantized levels) in the valence and conduction bands, and the nanoparticle progressively behaves similar to a giant atom. Nanosized semiconductor particles, which exhibit size-dependent optical and electronic properties, are called quantized particles or quantum dots (Kamat, 1995).

2.4.2 Activity of nano-photocatalysts

One of the main advantages of the application of nanosized particles is the increase in the band gap energy with decreasing particle size. As the size of a semiconductor particle falls below the critical radius, the charge carriers begin to behave mechanically quantum, and the charge confinement leads to a series of discrete electronic states. As a result, there is an increase in the effective band gap and a shift of the band edges. Thus by varying the size of the semiconductor particles, it is possible to enhance the redox potential of the valence band holes and the conduction band electrons.

However, the solvent reorganizational free energy for charge transfer to a substrate remains unchanged. The increasing driving force and the unchanged solvent reorganizational free energy are expected to lead to an increase in the rate constants for charge transfer at the surface. The use of nanosized semiconductor particles may result in increased photocatalytic activity for systems, in which the rate-limiting step is interfacial charge transfer. Hence, nanosized semiconductor particles can possess enhanced photoredox chemistry with reduction reactions, which might not otherwise proceed in bulk materials, being able to occur readily using sufficiently small particles. Another factor, which could be advantageous, is the fact that the fraction of atoms that are located at the surface of a nanoparticle is very large. Nanosized particles also have high surface area to volume ratios, which further enhances their catalytic activity. One disadvantage of nanosized particles is the need for light with a shorter wavelength for photocatalyst activation. Thus, a smaller percentage of a polychromatic light source will be useful for photocatalysis.
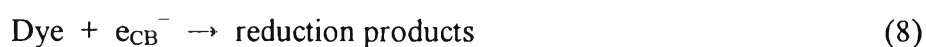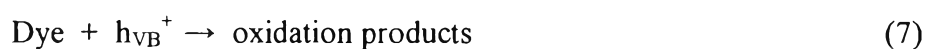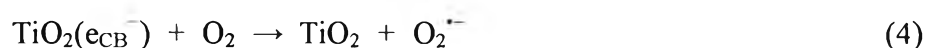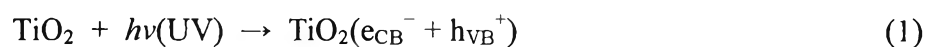
In large TiO_2 particles (Zhang *et al.*, 1998), volume recombination of the charge carriers is the dominant process and can be reduced by a decrease in particle size. This decrease also leads to an increase in the surface area, which can be translated as an increase in the available surface active sites. Thus, a decrease in particle size should also result in higher photonic efficiencies due to an increase in the interfacial charge carrier transfer rates. However, as the particle size is lowered below a certain limit, surface recombination processes become dominant, since firstly most of the electrons and holes are generated close to the surface, and secondly surface recombination is faster than interfacial charge carrier transfer

processes. This is the reason why there exists an optimum particle size for maximum photocatalytic efficiency.

2.5. Photocatalytic Decomposition Mechanisms
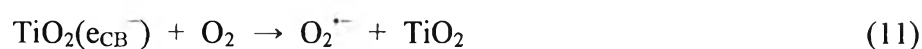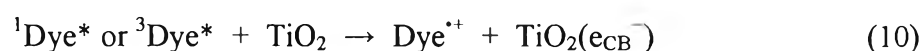
2.5.1 Photocatalytic oxidation

It is well established that conduction band electrons (e^-) and valence band holes (h^+) are generated when aqueous TiO_2 suspension is irradiated with light energy greater than its band gap energy (E_g, 3.2 eV). The photogenerated electrons can reduce the dye or react with electron acceptors, such as O_2 adsorbed on the Ti(III)-surface or dissolved in water, reducing it to superoxide radical anion $O_2^{\cdot-}$. The photogenerated holes can oxidize the organic molecule to form R^+ or react with OH^- or H_2O, oxidizing them into $OH^\cdot$ radicals. Together with other highly oxidant species (peroxide radicals), they are reported to be responsible for the heterogeneous TiO_2 photodecomposition of organic substrates as dyes. According to this, the relevant reactions at the semiconductor surface causing the decomposition of dyes can be expressed as follows:
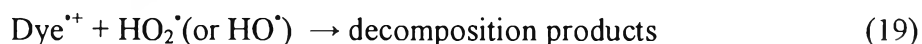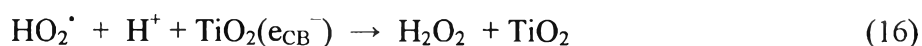
$$TiO_2 + h\nu(UV) \rightarrow TiO_2(e_{CB}^- + h_{VB}^+) \tag{1}$$

$$TiO_2(h_{VB}^+) + H_2O \rightarrow TiO_2 + H^+ + OH^\cdot \tag{2}$$

$$TiO_2(h_{VB}^+) + OH^- \rightarrow TiO_2 + OH^\cdot \tag{3}$$

$$TiO_2(e_{CB}^-) + O_2 \rightarrow TiO_2 + O_2^{\cdot-} \tag{4}$$

$$O_2^{\cdot-} + H^+ \rightarrow HO_2^\cdot \tag{5}$$

$$Dye + OH^\cdot,\ HO_2^\cdot,\ O_2^{\cdot-} \rightarrow decomposition\ products \tag{6}$$

$$Dye + h_{VB}^+ \rightarrow oxidation\ products \tag{7}$$

$$Dye + e_{CB}^- \rightarrow reduction\ products \tag{8}$$

The resulting $OH^\cdot$ radical, being a very strong oxidizing agent (standard redox potential of +2.8 V), as well as $HO_2^\cdot$ and $O_2^{\cdot-}$, can oxidize most of azo dyes to the mineral end-products. Substrates not reactive toward hydroxyl radicals are decomposed employing TiO_2 photocatalysis with rates of decay highly influenced by the semiconductor valence band edge position. The role of reductive pathways (Equation (8)) in heterogeneous photocatalysis has been envisaged also in the decomposition of several dyes but in a minor extent than oxidation.

2.5.2 Photosensitized oxidation

The mechanism of photosensitized oxidation (called also photoassisted decomposition) by visible radiation ($\lambda > 420$ nm) is different from the pathway implicated under UV light radiation. In the former case, the mechanism suggests that excitation of the adsorbed dye takes place by visible light to appropriate singlet or triplet states, subsequently followed by electron injection from the excited dye molecule into the conduction band of the TiO_2 particles, whereas the dye is converted to the cationic dye radicals ($Dye^{\cdot+}$) that undergoes decomposition to yield products as follows:

$$Dye + hv(VIS) \rightarrow {}^1Dye^* \text{ or } {}^3Dye^* \tag{9}$$

$${}^1Dye^* \text{ or } {}^3Dye^* + TiO_2 \rightarrow Dye^{\cdot+} + TiO_2(e_{CB}^-) \tag{10}$$

$$TiO_2(e_{CB}^-) + O_2 \rightarrow O_2^{\cdot-} + TiO_2 \tag{11}$$

$$Dye^{\cdot+} \rightarrow \text{decomposition product} \tag{12}$$

The cationic dye radicals readily react with hydroxyl ions undergoing oxidation via Equations (13) and (14) or interact effectively with $O_2^{\cdot-}$, $HO_2^{\cdot}$, or $HO^{\cdot-}$ species to generate intermediates that ultimately lead to CO_2 (Equations (15) – (19)).

$$Dye^{\cdot+} + OH^- \rightarrow Dye + HO^{\cdot} \tag{13}$$

$$Dye + 2HO^{\cdot} \rightarrow H_2O + \text{oxidation products} \tag{14}$$

$$O_2^{\cdot-} + H^+ \rightarrow HO_2^{\cdot} \tag{15}$$

$$HO_2^{\cdot} + H^+ + TiO_2(e_{CB}^-) \rightarrow H_2O_2 + TiO_2 \tag{16}$$

$$H_2O_2 + TiO_2(e_{CB}^-) \rightarrow HO^{\cdot} + HO^- + TiO_2 \tag{17}$$

$$Dye^{\cdot+} + O_2^{\cdot-} \rightarrow DO_2 \rightarrow \text{decomposition products} \tag{18}$$

$$Dye^{\cdot+} + HO_2^{\cdot}(\text{or } HO^{\cdot}) \rightarrow \text{decomposition products} \tag{19}$$
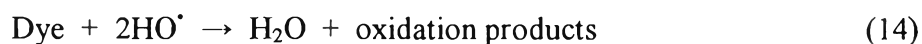
When using sunlight or simulated sunlight (laboratory experiments), it is suggested that both photooxidation or photosensitizing mechanism occurs during the irradiation, and both TiO_2 and the light source are necessary for the reaction to occur. In the photocatalytic oxidation, TiO_2 has to be irradiated and excited in a near-UV energy to induce charge separation. On the other hand, dyes rather than TiO_2 can be excited by visible light followed by electron injection into TiO_2 conduction band, which leads to photosensitized oxidation. It is difficult to conclude whether the photocatalytic oxidation is superior to the photosensitizing oxidation mechanism, but

the photosensitizing mechanism will help improve the overall efficiency and make the photobleaching of dyes using solar light more feasible.

2.6. Factors Influencing the Photocatalytic Decomposition

2.6.1 Effect of initial dye concentration

Yao *et al.* (2004) studied the decomposition of methyl orange by bismuth titanate, $Bi_4Ti_3O_{12}$, prepared by using the chemical solution decomposition (CSD) method. The results showed that with different methyl orange concentrations varied from 5 to 20 mg/l, the decomposition efficiency decreased with increasing concentration of methyl orange. The strong decrease in the observed rate constants with the increase in initial dye concentration was attributed to the significant absorption of light by the substrate in the same wavelength range of photocatalyst excitation. For increasing the initial methyl orange concentration, the photon flow reaching the photocatalyst particles decreased due to the fact that with increasing aliquots, photons are absorbed by the methyl orange molecules present in the solution and/or on the photocatalyst surface. Moreover, this dependence can also be related to the formation of several layers of adsorbed dye on the photocatalyst surface, which is higher at higher dye concentrations. The large amount of adsorbed dye inhibits the reaction of dye molecules with photogenerated holes or hydroxyl radicals because of the increased distance between reactants and photocatalysts.

2.6.2 Effect of TiO_2 loading

Whether in static, slurry, or dynamic flow reactors, the initial reaction rates were found to be directly proportional to photocatalyst concentration, indicating the heterogeneous regime. However, it was observed that above a certain level of concentration, the reaction rate even decreases and becomes independent of the photocatalyst concentration. Most of studies reported enhanced decomposition rates for photocatalyst loading up to 400–500 mg/l. Only a slight enhancement or decrease was observed when TiO_2 concentration further increased up to 2,000 mg/l. This can be rationalized in terms of availability of active sites on TiO_2 surface and the light penetration of photoactivating light into the suspension. The availability of active

sites increases with the suspension of catalyst loading, but the light penetration, and hence, the photoactivated volume of the suspension shrinks. Moreover, the decrease in the percentage of decomposition at higher photocatalyst loading may be due to deactivation of activated molecules by collision with ground state molecules. Agglomeration and sedimentation of the TiO_2 particles were observed elsewhere when 2,000 mg/l of TiO_2 was added to the dye solution. The crucial concentration depends on the geometry, the working conditions of the photoreactor, and the type of UV-lamp (power, wavelength). The optimum amount of TiO_2 has to be added in order to avoid unnecessary excess photocatalyst and also to ensure total absorption of light photons for efficient photodecomposition. This optimum loading of photocatalyst is also found to be dependent on the initial solute concentration (Konstantinou *et al.*, 2004).

2.6.3 Effect of solution pH

The heterogeneous photocatalysis has been found to be pH dependent. Yao *et al.* (2004) studied the decomposition of methyl orange by bismuth titanate, $Bi_4Ti_3O_{12}$, prepared by using the chemical solution decomposition (CSD) method. The results showed that with different initial pH values (1.22, 2.43, 5.18, 7.13, 10.2, and 12.7), the reaction rate increased at acidic pH but decreased at alkaline pH. The effect of pH on the decomposition of the pollutants is variable and controversial. The increase in decomposition rate at acidic pH was explained on the basis that at low pH, HO_2 radicals will form, and this will compensate for the effect of decreasing hydroxyl ion concentration. The decrease in decomposition rate at alkaline pH is assumed to be due to the anions and the highly negative charged oxide surface, and the decomposition would, thus, depend on diffusion of surface-generated $OH^{\bullet}$ towards the inside layer to the low concentration of methyl orange anion, a slower process than direct charge transfer.

2.6.4 Effect of light intensity and irradiation time

Oillis *et al.* (1991) reviewed the studies reported for the effect of light intensity on the kinetics of the photocatalysis process and stated that (i) at low light intensities (0–20 mW/cm^2), the rate would increase linearly with increasing light

intensity (first order), (ii) at intermediate light intensities beyond a certain value (approximately 25 mW/cm^2), the rate would depend on the square root of the light intensity (half order), and (iii) at high light intensities, the rate is independent of light intensity. This is likely because at low light intensity, reactions involving electron–hole formation are predominant, and electron–hole recombination is negligible. However, at increased light intensity, electron–hole pair separation competes with recombination, thereby causing lower effect on the reaction rate. It is evident that the percentage of decolorization and degradation increases with an increase in irradiation time. The reaction rate decreases with irradiation time since it follows apparent first-order kinetics, and additionally a competition for decomposition may occur between the reactant and the intermediate products. The slow kinetics of dye decomposition after certain time limit is due to:

- The difficulty in converting the N-atoms of dye into oxidized nitrogen compounds

- The slow reaction of short chain aliphatics with OH˙ radicals

- The short life-time of photocatalyst

because of active site deactivation by strong by-product adsorption (Konstantinou *et al.*, 2004).

2.6.5 Effect of H$_2$O$_2$

The influence of the strong oxidant species additives, such as H$_2$O$_2$, has been in some case controversial, and it appeared strongly dependent on substrate type and on various experimental parameters. Their usefulness should be accurately checked under each operative condition.

Yao *et al.* (2004) studied the decomposition of methyl orange and showed that with different concentrations of H$_2$O$_2$ (0, 0.1, and 1 mol/l), when the H$_2$O$_2$ was added, a significant increase in decomposition rate was noted for methyl orange decomposition but must be in the presence of photocatalyst and irradiation. Moreover, partial decomposition was observed for methyl orange under irradiation of the homogeneous systems in the presence of H$_2$O$_2$. In their work, the highest decomposition rate was achieved with 0.1 M H$_2$O$_2$ added. The added H$_2$O$_2$

contributed to the reactive radical intermediates (OH$^{\cdot}$) formed from the oxidants by reaction with the photogenerated electrons, which can exert a dual function: as strong oxidant themselves and as electron scavengers, thus inhibiting the electron–hole recombination at the semiconductor surface.

2.6.6 Effect of calcination temperature of photocatalyst

Yao *et al.* (2004) studied the effect of different calcination temperatures of photocatalyst for 5 min (400, 500, 600, and 700°C) at the same concentration of methyl orange (10 mg/l). The results showed that the photocatalytic activity of photocatalyst had no significant difference among the calcination temperatures of 400, 500, and 600°C, but the photocatalytic activity of the prepared photocatalysts was significantly reduced at higher calcination temperature (700°C).

Zhang *et al.* (2004) studied the photocatalytic activity of ZnO–SnO$_2$ for decomposition of methyl orange, and the effect of heat treating at different calcination temperatures was investigated (300, 350, 400, 450, 500, 600, 700, 800, and 900°C). The results showed that the degradation rate of methyl orange was increased with increasing calcination temperature except for 300°C because of the partial formation of crystallite oxides. With increasing calcination temperature, the size of crystallite oxides increases, contributing to the increase in photocatalytic activity. However, at temperatures higher than 700°C, the photocatalyst exhibited poor activity because of the negative effect of the coupled oxides.

2.6.7 Effect of calcination time of photocatalyst

Yao *et al.* (2004) also studied the effect of calcination time on the photocatalytic activity of the prepared bismuth titanate photocatalyst calcined at 600°C. The results showed that at 1 min of calcination time, the highest decomposition of methyl orange was obtained. While the rate constant increased with increasing calcination temperature, but at calcination time of 5 min, the rate constant reached the highest value because at the higher calcination time of 10 min, the sintering of photocatalyst material occurred.

2.7. Porous Materials

The classification of pores according to size has been under discussion for many years, but in the past, the terms "micropore" and "macropore" have been applied in different ways by physical chemists and some other scientists. In an attempt to clarify this situation, the limits of size of the different categories of pores included in Table 3 have been proposed by the International Union of Pure and Applied Chemistry (IUPAC), (Ishizaki *et al.*, 1988 and Rouquerol *et al.*, 1999). As indicated, the "pore size" is generally specified as the "pore width", i.e. the available distance between the two opposite walls. Obviously, pore size has a precise meaning when the geometrical shape is well defined. Nevertheless, for most purposes, the limiting size is that of the smallest dimension, and this is generally taken to represent the effective pore size. Micropores and mesopores are especially important in the context of adsorption.

Table 2.3 Definitions about porous solids

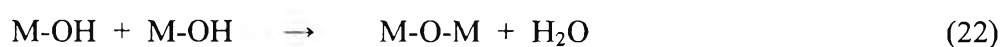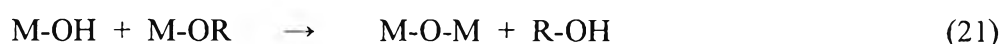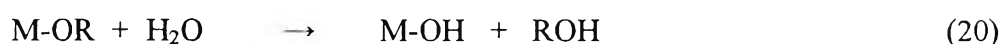| Term	Definition
Porous solid	Solid with cavities or channels which are deeper than they are wide
Micropore	Pore of internal width less than 2 nm
Mesopore	Pore of internal width between 2 and 50 nm
Macropore	Pore of internal width greater than 50 nm
Pore size	Pore width (diameter of cylindrical pore or distance between opposite walls of slit)
Pore volume	Volume of pores determined by stated method
Surface area	Extent of total surface area determined by given method under stated conditions

According to the IUPAC classification, porous materials are regularly organized into three categories on a basis of predominant pore size as follows:

- Microporous materials (pore size < 2 nm) include amorphous silica and inorganic gel to crystalline materials, such as zeolites, aluminophosphates, gallophosphates, and related materials.

- Mesoporous materials (2 nm ≤ pore size ≤ 50 nm) include the M41S family (e.g. MCM-41, MCM-48, MCM-50, and etc.) and other non-silica materials synthesized via intercalation of layered materials, such as double hydroxides, metal (titanium, zirconium) phosphates, and clays.

- Macroporous materials (pore size > 50 nm) include glass-related materials, aerogels, and xerogels.

Nowadays, micro- and mesoporous materials are generally called "nanoporous materials". Particularly, mesoporous materials are remarkably very suitable for catalysis applications, whereas the pores of microporous materials may become easily plugged during catalyst preparation if high loading is sought.

2.8. Sol-Gel Process

Several key techniques have been adopted to prepare mesoporous TiO_2, such as sol–gel process, hydrothermal process, and ultrasonic irradiation process. The sol–gel process is one of the versatile methods to prepare nano-sized mesoporous materials (Sreethawong et al., 2006). This technique does not require complicated instruments, such as in chemical vapor deposition method. It provides a simple and easy means of synthesizing nano-sized particles, which is essential for nano-catalysts (Wu et al., 2004). Besides, it is capable of producing photocatalysts with a high surface area. It involves the formation of metal-oxo-polymer network from molecular precursors, such as metal alkoxides, and subsequent polycondensation as follows:

$$M\text{-}OR + H_2O \longrightarrow M\text{-}OH + ROH \tag{20}$$

$$M\text{-}OH + M\text{-}OR \longrightarrow M\text{-}O\text{-}M + R\text{-}OH \tag{21}$$

$$M\text{-}OH + M\text{-}OH \longrightarrow M\text{-}O\text{-}M + H_2O \tag{22}$$

where M = Si, Ti, Zr, Al, and R = alkyl group. The relative rates of hydrolysis and polycondensation strongly influence the structure and properties of the resulting

metal oxides. Typically, sol-gel-derived precipitates are amorphous in nature, requiring further heat treatment to induce crystallization. The calcination process frequently gives rise to particle agglomeration and grain growth and may induce phase transformation (Wang and Ying, 1999).

Factors affecting the sol-gel process include the reactivity of metal alkoxides, pH of the reaction medium, water to alkoxide ratio, reaction temperature, and nature of solvent and additive. The water to alkoxide ratio governs the sol-gel chemistry and the structural characteristics of the hydrolyzed gel. High water to alkoxide ratios in the reaction medium ensures a more complete hydrolysis of alkoxides, favoring nucleation versus particle growth. In addition, an increase in water to alkoxide ratio leads to reduce the crystallite size of the calcined catalyst. An alternative approach to control the sol-gel reaction rates involves the use of acid or base catalyst. It was reported that for a system with a water to alkoxide ratio of 165, the addition of HCl resulted in the reduction of the crystallite size from 20 to 14 nm for materials calcined at 450°C. Besides, a finer grain size and a narrower pore size distribution with a smaller average pore diameter were also attained for the sample synthesized with HCl (Wang and Ying, 1999). The size of alkoxide group in alkoxides also plays an important role in controlling the particle size. The titanium alkoxide containing bulky groups, such as titanium amiloxide, reduces the hydrolysis rate, which is advantageous for the preparation of fine colloidal particles (Murakami et al., 1999).